Spectral Background-Subtracted Activity Maps

Carsten Denker [iD],[1] Meetu Verma [iD],[1] Alexander G.M. Pietrow [iD],[1] Ioannis Kontogiannis [iD],[1] and Robert Kamlah [iD][1,2]

[1]*Leibniz-Institut für Astrophysik Potsdam (AIP), An der Sternwarte 16, 14482 Potsdam, Germany*
[2]*Universität Potsdam, Institut für Physik und Astronomie, Karl-Liebknecht-Straße 24/25, 14476 Potsdam, Germany*

ABSTRACT

High-resolution solar spectroscopy provides a wealth of information from photospheric and chromospheric spectral lines. However, the volume of data easily exceeds hundreds of millions of spectra on a single observation day. Therefore, methods are needed to identify spectral signatures of interest in multidimensional datasets. Background-subtracted activity maps (BaSAMs) have previously been used to locate features of solar activity in time series of images and filtergrams. This research note shows how this method can be extended and adapted to spectral data.

1. INTRODUCTION

Initial ideas for extracting and visualizing temporal variations in time series were presented by Verma et al. (2012). The background-subtracted magnetic flux variation revealed a system of radial spokes in which moving magnetic features preferentially migrate, connecting a small sunspot to the adjacent supergranular cell boundary. The concept of a *Background-Subtracted Activity Map* (BaSAM) has been systematically introduced by Denker & Verma (2019) to study changes in the solar cycle, as seen in time series of full-disk UV images and photospheric magnetograms. Flare transients can be captured by BaSAMs (Pietrow et al. 2023), which, in combination with the Color Collapsed Plotting (CO-COPLOT, Druett et al. 2022) technique, reveal the temporal evolution of spectral features. Kamlah et al. (2023) extended the scope of BaSAMs to examine high-spatial-resolution data of pores and light-bridges and to imaging spectroscopy of the chromospheric Hα line. These results motivated this research note, which promotes BaSAMs as a tool for the analysis of multidimensional spectroscopic data (space, time, wavelength, and polarization state) from both ground-based solar observatories and space missions.

2. OBSERVATIONS

High-resolution spectroscopic data were obtained with the CHROMospheric Imaging Spectrometer (CHROMIS) at the 1-meter Swedish Solar Telescope (SST, Scharmer et al. 2003) on La Palma, Canary Islands, Spain. The target was a small sunspot in the trailing part of active region NOAA 12723 from 08:18 to 09:14 UT on 2018 September 30, which was also observed by Kuckein et al. (2021) and Vissers et al. (2022). The CHROMIS data are publicly available at the SST Data Archive[1] after image restoration with multi-object multi-frame blind deconvolution (MOMFBD, van Noort et al. 2005) and processing with the CRISPRED (de la Cruz Rodríguez et al. 2015) and SSTRED (Löfdahl et al. 2021) data reduction pipelines. The dataset consists of 205 spectral scans of the Ca II K $\lambda 3933$ Å and Hβ $\lambda 4861$ Å lines with 26 and 23 wavelength points, respectively. The CHROMIS bandpass has a FWHM of about 12 pm, and the plate scale of the detectors

Corresponding author: Carsten Denker
cdenker@aip.de

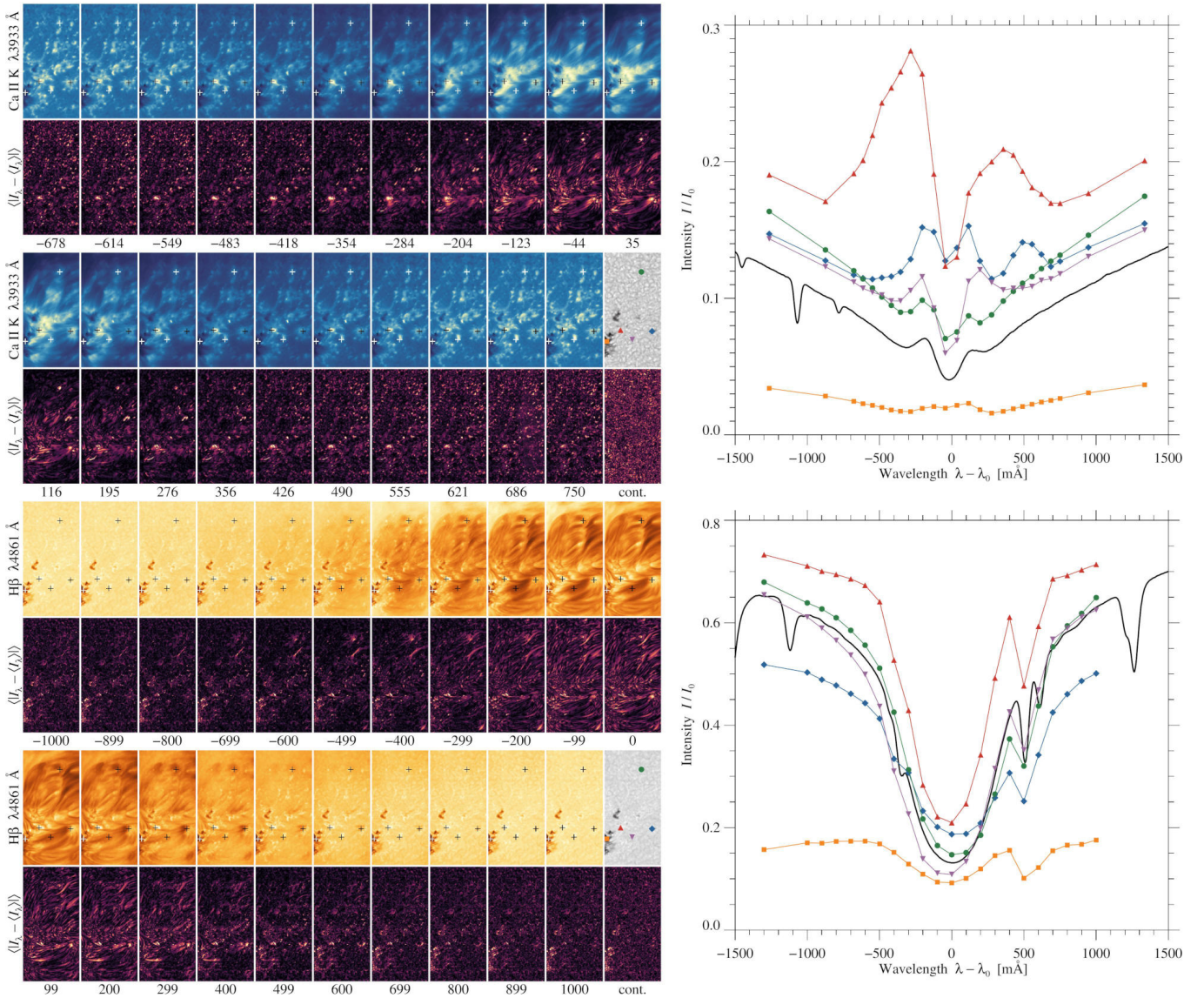[1] https://dubshen.astro.su.se/sst_archive/observations/237

Figure 1. Averaged spectral scans restored with MOMFBD of the chromospheric Ca II K (*blue*) and Hβ (*orange*) lines along with the corresponding spectral BaSAMs (*plasma color table*). The wavelength positions λ are given in milliångströms as measured from the line center λ_0. The two grayscale maps represent the averaged restored continuum images. The two insets on the right show FTS atlas spectra (*solid black*) with a spectral sampling of $\sim$2 mÅ of the Ca II K and Hβ lines and CHROMIS spectra at five locations, where the positions are marked by color-coded symbols in the continuum images and by plus signs in the spectral scans.

is 0.38″ pixel^{-1}. Since image rotation is present, the common field-of-view (FOV) is significantly reduced to 28.9″ × 58.8″ for the approximately 1-hour time series.

3. METHODS

The background-subtracted variation of a spectral quantity $I_\lambda(t)$, that is, filtergrams or slit-reconstructed spectral maps, within a time series is given by

$$\langle|I_\lambda - \langle I_\lambda\rangle|\rangle = \frac{1}{N}\sum_{i=1}^{N}|I_\lambda(t_i) - \langle I_\lambda\rangle|$$

$$\text{with}\quad \langle I_\lambda\rangle = \frac{1}{N}\sum_{i=1}^{N}I_\lambda(t_i),$$

(1)

where the subscript λ refers to the wavelength position in a spectral line scan, and t_i denotes the temporal position within the time series of spectral scans, and N is the total number of scans (cf., Denker & Verma 2019). Figure 1 aggregates approximately 3.67×10^8 spectra in 26 Ca II K and 23 Hβ background maps $\langle I_\lambda\rangle$ and BaSAMs $\langle|I_\lambda - \langle I_\lambda\rangle|\rangle$, where the angle brackets $\langle\ldots\rangle$ are shorthand for time averaging. Using 4×4-pixel binning kept the plot window of Fig. 1 to a manageable size.

4. RESULTS

Calculating spectral BaSAMs first produces an averaged spectral scan $\langle I_\lambda\rangle$ from a series of two-dimensional

narrow-band filtergrams. In this illustrative example persistent spectral features were associated with sunspots, pores, and an arch filament system (AFS), connecting opposite magnetic polarities in the lower part of the FOV. This system is best seen in Hβ line-core filtergrams. Bright footpoints mark the ends of horizontal dark fibrils connecting the sunspot on the left to a small pore embedded in bright plages on the right. Such regions associated with small-scale magnetic flux elements are best seen in the far wings of the Ca II K filtergrams, while Ca II K line-core filtergrams indicate chromospheric heating near the sunspot and pores associated with emerging flux.

The Ca II K line-wing BaSAMs $\langle|I_\lambda - \langle I_\lambda\rangle|\rangle$ clearly identify activity associated with the footpoints of the AFS, with the signal being stronger in the blue wing. In contrast, the right footpoint is more prominent in the Ca II K line-core BaSAMs. The central filament shows strong absorption but no activity features in the BaSAMs. However, strong variations delineate this filament, suggesting filament oscillations or flows aligned with the filament axis.

In addition to the AFS, minor activity occurs near small-scale active-region filaments in the upper-right part of the FOV. These variations appear as a small kernel in the Ca II K line-core BaSAMs and as filament-like features in the Hβ blue-wing and line-core BaSAMs. Overall, the morphology of the Ca II K and Hβ BaSAMs falls into three categories related to the outer and inner line wings and the line cores, reflecting the transition from the photosphere to the chromosphere.

The potential of spectral BaSAMs is summarized in the two plots in Fig. 1, where Ca II K and Hβ spectral lines for five locations are compared with the absolute disk-center intensity atlas spectrum (Neckel 1999) obtained with the McMath-Pierce Fourier Transform Spectrometer (FTS). Persistent intensity features in averaged spectral scans and regions with strong temporal variations, identified with spectral BaSAMs, served as objective criteria for selecting these locations. The averaged spectral profiles already show various spectral signatures, including blue- and red-shifts, line asymmetries, enhanced line wings, emission reversals, and (pseudo-)continuum and line-core intensities. These features, together with the averaged intensity and BaSAM values, can serve as a starting point for investigating the temporal evolution of spectra, for example, using machine learning techniques (e.g., Verma et al. 2021).

Facilities: SST – Swedish Solar Telescope, CHROMIS – Chromospheric Imaging Spectrometer

Software: BaSAMs (Denker & Verma 2019) – MOMFBD (van Noort et al. 2005) – CRISPRED (de la Cruz Rodríguez et al. 2015) – SSTRED (Löfdahl et al. 2021)

REFERENCES

de la Cruz Rodríguez, J., Löfdahl, M. G., Sütterlin, P., Hillberg, T., & Rouppe van der Voort, L. 2015, A&A, 573, A40, doi: 10.1051/0004-6361/201424319

Denker, C., & Verma, M. 2019, SoPh, 294, 71, doi: 10.1007/s11207-019-1459-x

Druett, M. K., Pietrow, A. G. M., Vissers, G. J. M., Robustini, C., & Calvo, F. 2022, RASTI, 1, 29, doi: 10.1093/rasti/rzac003

Kamlah, R., Verma, M., Denker, C., & Wang, H. 2023, A&A, 675, A182, doi: 10.1051/0004-6361/202245410

Kuckein, C., Balthasar, H., Quintero Noda, C., et al. 2021, A&A, 653, A165, doi: 10.1051/0004-6361/202140596

Löfdahl, M. G., Hillberg, T., de la Cruz Rodríguez, J., et al. 2021, A&A, 653, A68, doi: 10.1051/0004-6361/202141326

Neckel, H. 1999, SoPh, 184, 421, doi: 10.1023/A:1017165208013

Pietrow, A. G. M., Cretignier, M., Druett, M. K., et al. 2023, arXiv e-prints, doi: 10.48550/arXiv.2309.03373

Scharmer, G. B., Bjelksjo, K., Korhonen, T. K., Lindberg, B., & Petterson, B. 2003, in Proc. SPIE, Vol. 4853, Innovative Telescopes and Instrumentation for Solar Astrophysics, ed. S. L. Keil & S. V. Avakyan, 341–350, doi: 10.1117/12.460377

van Noort, M., Rouppe van der Voort, L., & Löfdahl, M. G. 2005, SoPh, 228, 191, doi: 10.1007/s11207-005-5782-z

Verma, M., Balthasar, H., Deng, N., et al. 2012, A&A, 538, A109, doi: 10.1051/0004-6361/201117842

Verma, M., Matijevič, G., Denker, C., et al. 2021, ApJ, 907, 54, doi: 10.3847/1538-4357/abcd95

Vissers, G. J. M., Danilovic, S., Zhu, X., et al. 2022, A&A, 662, A88, doi: 10.1051/0004-6361/202142087